Published online 7 February 2022

Nucleic Acids Research, 2022, Vol. 50, No. 4 ***2005–2018***
https://doi.org/10.1093/nar/gkac054

Klf4 methylated by Prmt1 restrains the commitment of primitive endoderm

Zhen-yu Zuo[1,†], Guang-hui Yang[1,†], Hai-yu Wang[2,†], Shu-yu Liu[1,†], Yan-jun Zhang[1], Yun Cai[1], Fei Chen[1], Hui Dai[1], Yi Xiao[2], Mo-bin Cheng[1,*], Yue Huang[2,*] and Ye Zhang[1,*]

[1]State Key Laboratory of Medical Molecular Biology, Department of Biochemistry and Molecular Biology, Institute of Basic Medical Sciences, Chinese Academy of Medical Sciences & Peking Union Medical College, Beijing 100005, China and [2]State Key Laboratory of Medical Molecular Biology, Department of Medical Genetics, Institute of Basic Medical Sciences, Chinese Academy of Medical Sciences & Peking Union Medical College, Beijing 100005, China

Received November 12, 2021; Revised January 11, 2022; Editorial Decision January 15, 2022; Accepted January 25, 2022

ABSTRACT

The second cell fate decision in the early stage of mammalian embryonic development is pivotal; however, the underlying molecular mechanism is largely unexplored. Here, we report that Prmt1 acts as an important regulator in primitive endoderm (PrE) formation. First, Prmt1 depletion promotes PrE gene expression in mouse embryonic stem cells (ESCs). Single-cell RNA sequencing and flow cytometry assays demonstrated that Prmt1 depletion in mESCs contributes to an emerging cluster, where PrE genes are upregulated significantly. Furthermore, the efficiency of extraembryonic endoderm stem cell induction increased in Prmt1-depleted ESCs. Second, the pluripotency factor Klf4 methylated at Arg396 by Prmt1 is required for recruitment of the repressive mSin3a/HDAC complex to silence PrE genes. Most importantly, an embryonic chimeric assay showed that Prmt1 inhibition and mutated Klf4 at Arg 396 induce the integration of mouse ESCs into the PrE lineage. Therefore, we reveal a regulatory mechanism for cell fate decisions centered on Prmt1-mediated Klf4 methylation.

INTRODUCTION

Mammalian embryogenesis occurs through an ordered process (1,2)). During mouse early embryo development, the first cell fate decision results in the emergence of two cell lineages, the inner cell mass (ICM) and trophectoderm (TE) (3,4), which are specified at the molecular level by Oct4/Pou5f1 and Cdx2, respectively (5–7). Subsequently, ICM segregates into the epiblast (EPI) and primitive endoderm (PrE) at E4.5, which is termed the second cell fate decision (1,8). The process of PrE and EPI specification within the ICM is beginning to be elucidated. To be more specific, Gata6 and Nanog, the key factors for ICM segregation, become heterogeneously expressed at the early blastocyst stage (9–11). Subsequently, these factors progressively become mutually exclusive in their expression, which marks the initiation of lineage segregation (11). Embryonic stem (ES) cells with high Nanog expression and low Gata6 expression acquire an EPI fate (9,12,13), while PrE lineage commitment requires the repression of Nanog (14) and sequential activation of Gata6 (15–17), Sox17 (18), Gata4 (19) and Sox7 (20). Overall, Gata6 and Nanog, the earliest markers of the PrE and EPI lineages, respectively, act near the top of the hierarchy regulating PrE development (14). However, the molecular mechanisms governing the specification of PrE and EPI, or rather regulating the switch of Gata6 and Nanog expression, are still poorly understood.

Epigenetic modifications have been proven to be essential for cell fate determination and early embryo development (21,22). Protein arginine methylation catalyzed by enzymes in the protein arginine methyltransferase (PRMT) family is a prevailing posttranslational modification that functions as an epigenetic regulator of transcription in multiple cellular processes, including cell fate decisions (23–26). In the PRMTs family, Prmt4/Carm1 regulates cell fate decisions early in the four-cell stage by methylating histone H3R26 and activating Sox21 expression in mouse ESCs (27,28). We previously reported that Sox2 is methylated by Carm1

*To whom correspondence should be addressed. Tel: +86 106 915 5939; Fax: +86 106 526 9665; Email: yezhang@ibms.pumc.edu.cn
Correspondence may also be addressed to Yue Huang. Email: huangyue@pumc.edu.cn
Correspondence may also be addressed to Mo-bin Cheng. Email: mobincheng@genmedicn.com
†The authors wish it to be known that, in their opinion, the first four authors should be regarded as joint First Authors.
Present addresses:
Zhen-yu Zuo, NICHD, NIH, Bethesda, MD, USA.
Guang-hui Yang, NIDDK, NIH, Bethesda, MD, USA.
Hai-yu Wang, Leiden University Medical Center, Leiden, The Netherlands.
Fei Chen, Max Planck Institute for Molecular Biomedicine, Muenster, Germany.

at R113, leading to its self-association and activation (29). Prmt5 can methylate histone H2A to repress differentiation genes in ES cells and is crucial for early mouse development (30). Prmt6 regulates both pluripotency genes and differentiation markers to participate in the maintenance of ES cell identity (31). Although Prmt1 provides the bulk of the protein arginine methylation activity within cells (32,33) and Prmt1-null mice die at E6.5 (34), little is known about the role of Prmt1 in early embryonic development.

In this study, we report that Prmt1 depletion in mouse ESCs leads to the emergence of a cluster with the properties of PrE progenitor. Prmt1 interacts with and arginine-methylates Klf4, a key pluripotency factor. Methylated Klf4 is essential for the recruitment of the repressive mSin3a/HDAC complex to silence the expression of PrE genes in mouse ESCs. Both Klf4 R396 mutation and the enzymatic inactivation of Prmt1 derepress PrE genes, followed by a tendency toward the development of extraembryonic endoderm stem (XEN) cells. Moreover, a Prmt1 enzymatic inhibitor and Klf4 R396A mutant promote the formation of PrE *in vivo*. Our data reveal a novel molecular mechanism controlling second cell fate determination in embryogenesis mediated by the enzymatic function of Prmt1.

MATERIALS AND METHODS

Antibodies

The antibodies used in this study were purchased from the following sources: Millipore (Billerica, MA): ASYM25 (09-814), HP1 (MAB3448), histone H3 (06-755), H3ac (06-599), H3K4me3 (07-473), H3K9me2 (07-441), H3K9me3 (07-442), H3K27me3 (07-449), H4 (05-858), H4ac (06-598), Prmt1 (07-404) and Sox2 (AB5603); Santa Cruz Biotech (Santa Cruz, CA): actin (sc-47778), c-Myc (sc-40, sc-789), GAPDH (sc-166574), Gata4 (sc-9053), Gata6 (sc-9055), GST (sc-138), mSin3a (sc-994), Oct4 (sc-5279) and p300 (sc-32244); Cell Signaling Technology (Danvers, MA): HDAC1 (2062), HDAC2 (2545s) and KLF4 (4038); Abcam (Cambridge, UK): H3R17me2 (ab412); Sigma (St. Louis, MO): FLAG (F3165); MBL (Japan): FLAG (PM020); Active Motif (Carlsbad, CA): H4R3me2a (39705); R&D Systems (Minneapolis, MN): KLF4 (AF3158); and Bethyl Laboratories (Montgomery, TX): Nanog (A300-397A).

A specific monoclonal antibody against Klf4-R396me2a was generated by Absea Biotechnology Ltd (Beijing, China) using synthesized peptide CGRRSWPRKRTATHT, corresponding to residues aa 387–402 of Klf4, as an antigen.

Plasmids and transfection

Mouse Prmt1 cDNA was amplified by PCR from P19 cells and cloned into the pcDNA6-FLAG vector. Full-length mouse KLF4 in the pCMV-Tag2B vector was a kind gift from Dr Wen-ji Dong (PUMC). The Prmt1 mutant (E153Q) and point mutants (R to K or R to A) of Klf4 at R 387, 389, 390, 394 and 396 were generated by CR-based site-directed mutagenesis. KLF4 wild-type and mutants were cloned into the prokaryotic expression vector pGEX-4T-1 and the eukaryotic expression vector pCMV-Tag3B with a Myc-tag. All the expression plasmids above were cloned into the PyCAG-FLAG-HA vector for transfection into ESCs, and all constructs were verified by DNA sequencing. Transfection was carried out using Lipo3000 transfection reagent (Invitrogen), according to the manufacturer's instructions.

Generation of Prmt1-KO E14 cell line

The Prmt1-KO E14 cells were generated using CRISPR-Cas9 as described previously (35). Four pairs of sgRNAs targeting exon3, exon4, exon5, and exon6 separately were designed by http://crispr.mit.edu/. The sequence of sgRNA is: Exon3-sense: 5′-CACCGTAGTGAGAAGCCCAACGCTG-3'; Exon3-antisense: 5′-AAACCAGCGTTGGGCTTCTCACTAC-3′; Exon4-sense: 5′-CACCGCGGGGGCCCGCAAGG TTATT-3′; Exon4-antisense: 5′-AAACAATAACCTTG CGGGCCCCCGC-3′; Exon5-sense: 5′-CACCGCACAG CATAATCGGAGATAC-3′; Exon5-antisense: 5′-AA ACGTATCTCCGATTATGCTGTGC-3′; Exon6-sense: 5′-CACCGCAACACCGTGCTGCACGCTC-3′; Exon6-antisense: 5′-AAACGAGCGTGCAGCACGGTGTTGC-3′. Two pairs of control sgRNA, which are not able to target any position in mouse genome, were: control1-sense: 5′-CACCGCTTACAATCGTCGGTCCAAT-3′; control1-antisense: 5′-AAACATTGGACCGACGATTGTAAG-3′; control2-sense: 5′-CACCGGCGTGCGTCCCGGGT TACCC-3′; control2-antisense: 5′-AAACGGGTAACC CGGGACGCACGC-3′. The oligos of sgRNA were synthesized then ligated into pX330. In control group, control1-px330 and control2-px330 were cotransfected in E14 cells together with a puromycin-resistant plasmid. In parallel, exon3-px330 and exon5-px330 were cotransfected in one dish of E14, termed group1; Exon4-px330 and exon6-px330 were in another dish of E14, termed group2. After puromycin selection, single colonies from control group, group1 and 2 were picked. After expansion, Prmt1-KO cells were identified by genotyping, qPCR and western blot, named as Prmt1-KO1 and Prmt1-KO2 cell line individually. In Prmt1-KO1 cells, the two alleles of Prmt1 are identical. There is 2 bp-deletion in Exon3, which leads to a frame shift and the appearance of a stop codon. In Prmt1-KO2 cells, the sequence of two alleles of Prmt1 after gene editing is not the same. On one allele, there is 23-bp deletion in Exon4. On the other allele, the fragment between Exon4 and Exon6 is inverted and reinserted into the genome (Supplementary Figure S1D). Both of the two alleles are disrupted successfully.

Cell culture and XEN induction

Mouse E14 ES cells (a kind gift from Prof. Guo-hong Li from the Institute of Biophysics, Chinese Academy of Science) were cultured on plates coated with 0.1% gelatin (Millipore) under feeder-free conditions with 5% CO_2 at 37°C. The ESC medium was prepared from Knockout DMEM (Gibco), with 15% fetal bovine serum (FBS, Gibco), 0.1 mM β-mercaptoethanol (Millipore), 2 mM GlutaMax (Gibco), 0.1 mM MEM nonessential amino acids (Gibco) and 1000 U/ml LIF (Millipore). HEK293T cells were cultured in DMEM supplemented with 10% FBS and maintained at 37°C with 5% CO_2.

The ESCs was induced to develop into XEN cells following a previous protocol (36). In brief, mouse ESCs were cultured in standard XEN medium: advanced RPMI 1640 (Gibco) with 15% (vol/vol) FBS (Gibco) and 0.1 mM-mercaptoethanol (Gibco). Then, the fresh cXEN derivation medium was changed to a solution of standard XEN medium supplemented with 0.01 μM all-trans retinoic acid (Sigma) dissolved in DMSO plus 10 ng/ml activin A. After induction, the cells were identified by qPCR and immunofluorescence assays.

Construction of Klf4 R396A point mutation Ab2.2 ES cell line

The original 748 bp wild type donor template was amplified from the mouse genome with the following primers: W1: forward primer (Fw): CCAGGACTACCCCTACACTGA; W2: reverse primer (Rv): TACCGCCACAGTTTTGCATT. The sequence was cloned into the pMD 18-T vector. The G to A mutation was generated through PCR with the primers: M1: G>A Fw: CGTGGCCCCGGAAACGTA CAGCCACCCACAC; M2: G>A Rv: GTGTGGGTGG CTGTACGTTTCCGGGGCCACG. The Dpn I enzyme (NEB, R0176L) was used to clear the original vector. The mutated donor template was amplified with the W1 and W2 primers and the PCR product was purified using GeneJET PCR Purification Kit (Thermo, K0702).

For the construction of the cell line, sgRNAs were designed as followed: sgRNA1: GATTGAAGTTGACC CCACTT; sgRNA2: GGAACCAGCACTGTGGAGGA. sgRNAs were cloned into the pX330-U6-Chimeric BB-CBh-hSpCas9 vector. For targeting, cells were disassociated into single cells and 1×10^7 cells were electroporated with a mixture of 2 μg CRISPR plasmid together with 2 μg donor template and 0.5 μg PGG134 vector (for the drug selection). Cells were plated after electroporation and treated with 150 μg/ml hygromycin for 3 days. 2000–3000 cells after treatment were plated onto 10 cm dish, and 96 single colonies were picked up to the wells of a 96-well plate individually. After expansion, genomic DNA was extracted and PCR was performed with the final detection primers: D1: Fw: CCTAGAGGCCCATTTGAGCG; D2: Rv: TACCGCCACAGTTTTGCATTG. The PCR products were further validated by Sanger sequencing. The correctly mutated cells were expanded and microinjected into the mouse blastocysts as described below.

Chimeric assay of mouse ES cells *in vivo*

In order to detect the *in vivo* contribution of the ES cells, Ab2.2 (GFP2AtdT) cell line (37) was used to carry on the chimeric assay. The cells were injected into blastocysts three days after passaging, one group of which was also pretreated with Prmt1 inhibitor at 10 μM for 24 h before injection. For microinjection, ES cells were trypsinized by 0.05% trypsin–EDTA, and centrifuged at 1200 rpm for 3 min. The cell pellets were resuspended and replaced into a six-well plate for 30 min to subside MEF cells. The tube containing cells was placed in the ice during the process of microinjection. Recipient blastocyst embryos were collected from super-ovulated female ICR mice at 3.5 days post-coitum (dpc). Ten digested ES cells were injected into one blastocyst, then 10–15 injected embryos were transferred to the uterus of one 2.5 dpc pseudo-pregnant ICR female. The transplanted embryos were observed at the indicated time points. The fluorescent signals of 6.5d and 12.5 days embryos were detected using fluorescence stereo microscope (Leica M205FA). Besides, 6.5 days embryos were fixed in 4% PFA and observed by Zeiss LSM780. The Ab2.2 cells with or without Klf4R396A mutation was used to perform the chimeric assay as above described. The transplanted embryos at 6.5 days were fixed in 4% PFA and observed by Zeiss LSM780.

All mouse experimental protocols were approved by the Institutional Animal Care and Use Committee of Peking Union Medical College & Chinese Academy of Medical Sciences. All animal care and experimental methods were carried out in accordance with the ARRIVE guidelines for animal experiments. All the mice used in this study were fed in Specific Pathogen Free (SPF) facilities.

Immunofluorescence (IF)

The ES cells were seeded on coverslips coated with 0.1% gelatin in six-well plates for 24 h. The cells were fixed with 4% formaldehyde for 10 min at room temperature, and the coverslips were washed two times in PBS. Then, the cells were permeabilized with 0.25% Triton-X-100 in PBS for 10 min and blocked with 1% BSA in PBS for 1 h. The cells were then incubated at room temperature with primary antibody for 1 h and with FITC-conjugated or TRITC-conjugated secondary antibody for an additional 1 h. After being washed twice in PBS and air-dried, the coverslips were mounted in anti-fade reagent with DAPI (Invitrogen). Fluorescence was detected using a Zeiss (LSM780) microscope at appropriate wavelengths.

Immunofluorescence of blastocysts for 3.5 dpc were performed as a protocol (38) with some modifications. The blastocysts of 3.5 dpc were collected and cultured in KSOM (Millipore, MR-020P-5F) medium in a humidified incubator under 5% CO2 at 37°C with or without 10 μM Prmt1 inhibitor. After 24h, the blastocysts were rinsed in PBS-BSA (4 mg/ml BSA) for three times and fixed in 4% PFA in PBS for 10 min at RT. All the steps were performed in the 35 mm dish with 10 mm bottom well (In Vitro Science, D35-10-1.5-N), the bottom well was coated with a layer of 1% agar in 0.9% NaCl. Fixed blastocysts were then rinsed in PBX (0.1% Triton X-100 in PBS) for 5 min and permeabilized in permeabilization solution (0.5% Triton-X, 100 mM glycine in PBS) for 5 min at RT. Blastocysts were then rinsed in PBX and blocked for 30 min in the blocking solution (20% FBS with Pen-Strep in PBS). The blastocysts were then incubated in PBX containing the primary antibodies of Nanog (1:200 Invitrogen, 14-5761-80) and Gata6 (1:200 R&D, AF1700) at 4°C overnight. A layer of mineral oil was used to prevent evaporation. After blocking for 30 min, blastocysts were incubated with secondary antibodies (1:500, Donkey anti-Rabbit IgG (H+L) Highly Cross-Adsorbed Secondary Antibody, Alexa Fluor 488, Life Technology, A-21206; Donkey anti-Goat IgG (H+L) Cross-Adsorbed Secondary Antibody, Alexa Fluor 647, Invitrogen, A-21447) and Hochest 33342 (Sigma, B2261) at 4°C

for 1 h. Embryos were then seeded into PBS-BSA drops in the 35 mm dish and covered by mineral oil before imaging with Zeiss LSM780.

Co-immunoprecipitation (Co-IP) and western blotting

Co-IP analyses were performed as previously described (39).

GST pulldown assay

Full-length mouse KLF4 and truncated KLF4 constructs were expressed in *Escherichia coli* (BL21 DE3) and purified using glutathione-sepharose. GST, GST-KLF4 and truncated KLF4 were bound to glutathione-sepharose. FLAG-tagged Prmt1 was transfected into HEK293T cells, followed by incubation with bacterially expressed GST-KLF4 fusion protein sepharose in RIPA lysis buffer for 4 h at 4°C. The beads were washed 3 times using RIPA and boiled with 2 × SDS loading buffer for SDS-PAGE.

Peptide pulldown assay

We designed and synthesized two biotinylated peptides corresponding to Klf4 protein (388–401aa), one of them has dimethylation modification at R396, another unmodified peptide of the same size served as a negative control (R396Me2a/R396). Biotinylated peptides were pre-bound to the immobilized streptavidin-magnetic beads.1 mg peptide were dissolved in 4 ml phosphate buffer saline (PBS). Aliquots (400 μl) of the beads were washed three times in 1 ml phosphate buffered saline (PBS)/0.1% TritonX-100, each time centrifuging statically on the magnetic rack. The 400 μl soluble peptide (100 μg) was added to the 400 μl washed beads and the reactions were incubated overnight at 4°C with rotation. The streptavidin beads were separated from the unbound peptides by washing three times with PBS/0.1%TritonX-100. The streptavidin-bound peptides were suspended in PBS (400 μl) to prepare 50% of the storage solution, it could be stored at −20°C. 3 μg (20 μl) HDAC1 protein (Active Motive, 33120006) was added to 20 μl each streptavidin-bound peptide solution. The reactions were incubated with rotation overnight at 4°C. The beads were washed three times. Then, loading buffer was added, and the beads were boiled at 100°C for 5 min and analyzed by SDS-PAGE. In addition, 0.03 μg HDAC1 protein was taken as the positive control group (1% input).

In vitro methylation assay and MS analysis

FLAG-Prmt1 and Prmt1m (E153Q) were expressed in HEK293T cells and immunoprecipitated with anti-FLAG M2 agarose beads (Sigma) and then eluted with excess FLAG peptides. GST-KLF4 and mutants were expressed in *E. coli* (BL21 DE3), purified using glutathione-sepharose, and eluted with glutathione. Purified Klf4 was incubated with WT Prmt1 or Prmt1m in methyltransferase buffer (50 mM Tris [pH 8.0], 1 mM PMSF, 0.5 mM DTT) along with 1 μCi of [^{3}H] *S*-adenosylmethionine (SAM) or unlabelled 100 μM SAM at 37°C for 1 h. Reactions were stopped by adding 2× SDS-PAGE sample buffer, followed by heating at 100°C for 5 min. Samples were resolved by SDS-PAGE and stained with CBB. The destained gels were soaked in EN^{3}HANCE (PerkinElmer) according to the manufacturer's instructions and visualized by fluorography. Methylated substrates with unlabelled SAM were sent to PTM Biolabs (Hangzhou, China) for MALDI-TOF MS analysis.

Real-time quantitative RT-PCR (RT-qPCR)

Total RNA was purified with TRIzol reagent (Invitrogen) according to the manufacturer's instructions. Two micrograms of total RNA were used for cDNA synthesis with a reverse transcription kit (Promega). Quantitative real-time PCR was performed using the SYBR premix kit (Promega), and the primer sequences used are listed in Supplemental Table S2. Gene expression was quantified by the comparative CT method and normalized to actin expression. Values are expressed as the mean ± SD. The experiments were repeated at least three times, and statistical analysis was performed on the individual experimental sets.

RNA-Seq and analysis

Approximately 5 × 10^6 E14 cells were used for each RNA-Seq experiment. The cells were washed with PBS and then lysed in 1 ml of TRIzol reagent (Invitrogen). Total RNA was extracted following the manufacturer's instructions and dissolved in RNase-free water. A Ribo-Zero Magnetic Gold Kit (epicenter) was used to deplete ribosomal RNA within RNA samples according to the manufacturer's protocol. The Ion Total RNA-Seq Kit v2 (Thermo Fisher Scientific) was used to prepare sequencing libraries. A total of 40–80 million reads were generated for each sample on an Ion Proton sequencing machine with an average length of 105 bp. Read quality was examined using FastQC v0.11.2. The sequencing reads were first aligned with the mouse mm10 (GRCm38.78) reference genome using RNA-STAR v2.4.0j (40). Unaligned reads were then aligned again with Bowtie2 v2.2.4. Cufflinks v2.2.1 was used to calculate RPFMs of different genes and determine expression differences between groups. The data were visualized with IGV 2.3.40. All sequencing data were deposited in the GEO database (GSE124920). Weighted correlation network analysis (WGCNA) was used of co-expression analysis and the gene grouping for RNA-Seq analysis (41).

Single-cell RNA-Seq

Mouse ES cells were dissociated with TrypLE. Single ES cells were washed and diluted in PBS to a final concentration of 600 cells/μl. More than 95% cell viability was confirmed with trypan blue staining. 17.4 μl cell suspension was used to prepare single cell RNA-Seq library following ChromiumTM Single Cell 3′ Reagent Kits (Ver2) user guide. Sequencing was performed on Illumina HiSeq X ten in Rapid mode for pair end 150 bp (PE150) read length. The Seurat [https://satijalab.org/seurat/] package for cell normalization and cell filtering was applied considering the MT percentage (MT% < 20%). PCA and tSNE analysis were used to describe relationship between single cells. Graphcluster and *K*-mean were utilized for cell clustering and based on the marker gene achieved some cluster

was combined. The Wilcox rank sum test was then used for marker gene analysis. Based on the rds file analyzed by the Seurat package, including clustering and cell marker identification, Monocle2 (42) was utilized for pseudotime analysis; the state of each cell was analysed, and single cells were placed in clusters along a trajectory according to a biological process, such as cell differentiation by taking advantage of individual cell's asynchronous progression of those processes. RNA velocity analysis was applied based on the mapped file of the filtered data (43). The locus file was calculated, and the figure was constructed based on the Seurat clustering result.

ChIP-qPCR assays and ChIP/re-ChIP analysis

The ChIP assays were performed as described previously (39). The primers used for the qPCR assay of Gata4 and Gata6 are listed in Supplemental Table S3. The percentage of ChIP DNA relative to the input was calculated and expressed as the mean ± SD of three independent experiments.

For ChIP/re-ChIP analysis, ESCs were first transiently transfected with FLAG-KLF4 or the R/K mutant of the Klf4 expression plasmid. The sonicated cells were immunoprecipitated using anti-FLAG M2 beads (Sigma). Aliquots of the first ChIPed chromatin (1st ChIP) were reverse cross-linked to obtain DNA for qPCR assays or were saved for re-IP using antibodies specific for mSin3a, HDAC1, HDAC2 or p300 for re-ChIP assays (2nd ChIP). The primers are listed in Supplemental Table S3.

DNase I sensitivity assay

The DNase I sensitivity assay was carried out as previously described (39). Briefly, a total of 1×10^7 wild-type or Prmt1 knockout E14 cells were used. Aliquots of 10 μg DNA were purified for qPCR using the primers listed in Supplemental Table S3.

Flow cytometry assays

Mouse ES cells were dissociated into single cells by incubation with TrypLE (Gibco). The ells were washed and diluted in PBS. Staining was carried out using Foxp3/Transcriptn Factor Staining Buffer Set Kit (eBioscience) according to the manufactural protocol. The cells were stained with the following antibodies: anti-Nanog-APC (Cat#130-104-480, Miltenyi Biotec), anti-Gata6-PE (Cat#26452, Cell Signaling Technology), Isotype control APC (Cat#130-104-615, Miltenyi Biotec) and Isotype control PE (Cat#5742, Cell Signaling Technology). The stained cells were analyzed on a C6 flow cytometer (BD). Data were analysed with FlowJo software.

RESULTS

Prmt1 depletion leads to the emergence of progenitors of PrE

To investigate the effects of Prmt1 in mouse ESCs, Prmt1 knockout E14 cell lines (KO-1 and KO-2) were generated by using CRISPR-Cas9 technology. Depletion of Prmt1 and the possibility of off-target effects were shown in Supplementary Figure S1 and Supplementary Table S1. Alkaline phosphatase (AP) staining and teratoma formation assays indicated that Prmt1 depletion did not significantly affect the pluripotency of mESCs (Supplementary Figures S2A and B). RT-qPCR and western blot assays showed that Prmt1 depletion did not substantially change the expression of Oct4, Sox2 and Klf4 genes, while a reduction in Nanog was observed in Prmt1 KO cells (Supplementary Figure S2C-D). Furthermore, RNA-Seq showed that 2363 genes were downregulated after Prmt1 depletion, while 2499 genes were upregulated (Supplementary Figure S2E). GO analysis according to the differentially expressed genes (DEGs) revealed significant enrichment of upregulated genes involved in developmental processes (Supplementary Figure S2F). To our surprise, weighted gene co-expression network analysis (WGCNA) (41) showed that upregulation of PrE genes, including *Gata6*, *Gata4*, *Dab2*, *Foxa2* and *Pdgfra*, exhibited the closest relationship with Prmt1 depletion (Figure 1A). RT-qPCR assays confirmed that the expression of *Gata4* and *Gata6* was significantly increased in Prmt1 KO cells (Figure 1B). Furthermore, immunostaining with antibodies specific for Gata6 (green) and Nanog (red) in WT and *Prmt1* KO cells showed that endogenous Gata6 was induced in some *Prmt1* KO cells, conversely, the Nanog level was reduced (Figure 1C). Interestingly, Gata6 was heterogeneously expressed in *Prmt1* KO cells, which suggested that Prmt1 might be a regulatory factor for the heterogeneity of mESCs.

To explore the role of Prmt1 on the regulation of heterogeneity, single-cell RNA sequencing (scRNA-Seq) was performed using the Chromium system (10x Genomics) (44,45). scRNA-Seq data were obtained from 13 824 individual cells, including 5955 WT cells and 7869 *Prmt1* KO cells. Nonlinear dimensionality reduction was performed using *t*-distributed stochastic neighbor embedding (tSNE) by Seurat (*K*-means = 8), a visual analytics tool for integrated analysis, and eight clusters (1–8) were identified in the integrated data from WT and KO cells (Figure 1D and Supplementary Figure S3A). Among these clusters, clusters 1 and 2 were composed of only KO cells, while clusters 3–8 contained both WT and KO cells (Supplementary Figure S3B). Principal component analysis (PCA) based on pseudotime showed that cluster 1 was distant from the other clusters (Supplementary Figure S3C). The top 2000 of DEGs were analysed, and the results showed that cluster 1 was marked by upregulated expression of PrE marker genes, including *Gata4, Gata6, Sox17, Dab2, Amn, Foxa2, Sox7* and *Pdgfra,* while cluster 2 showing up-regulation of 2-Cell like markers, as *Zscan4c, Zscan4d* and *Zscan4f* (Figure 1E and Supplementary Figures S3D–F), while the expression of pluripotency genes *Oct4/Pou5f1, Sox2, Klf4, Esrrb* and *Sall4* were maintained in Prmt1 KO cells except for *Nanog*. Combined with data from the RNA-Seq and immunostaining experiments, the gene expression profile strongly suggested that the emerging cluster 1 from *Prmt1* KO cells was the progenitor of PrE cells. To gain insights into the gene expression dynamics and trajectory of this cluster, RNA velocity analysis was performed to predict gene expression changes in single cells (43,46,47). The results showed a strong directional flow toward progenitors

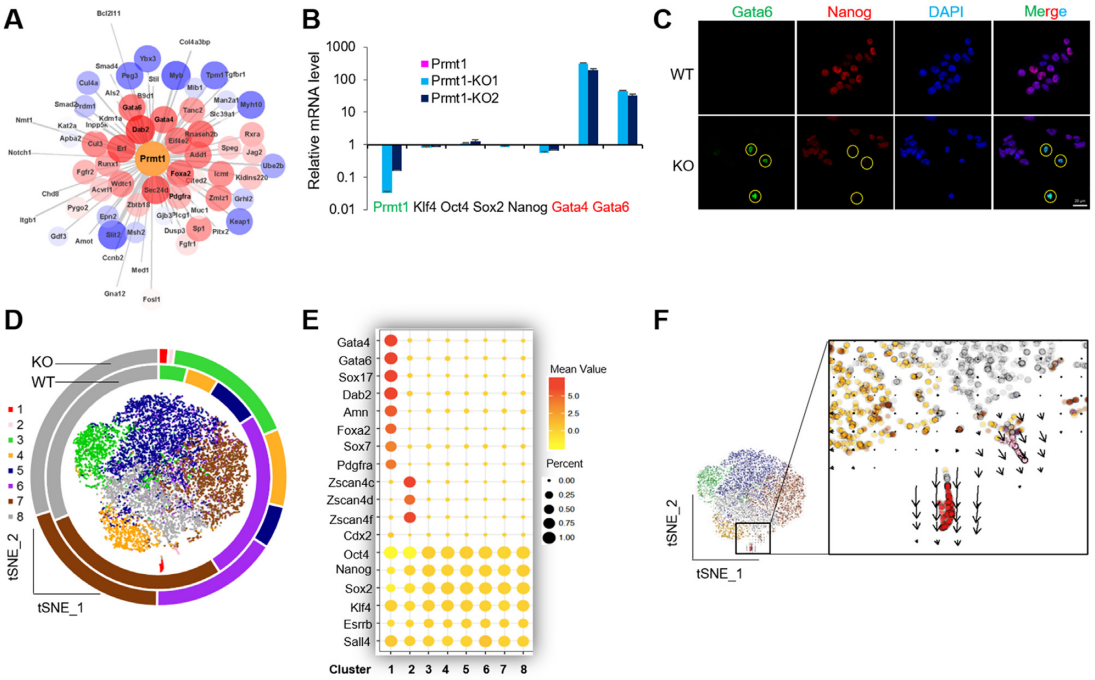

Figure 1. Prmt1 depletion leads to progenitor of PrE. (**A**) A WGCNA network was constructed based on Prmt1 and its related embryonic genes. Red indicates upregulation, and blue indicates downregulation. (**B**) RT-qPCR showing the expression of the indicated genes. (**C**) IF assays of endogenous Gata6 (green) and Nanog (red) in WT and Prmt1 KO cells. Nuclei were visualized with DAPI staining (blue). Yellow circles indicate Gata6-positive cells. (**D**) tSNE of 13 805 cells by scRNA-seq, include 5930 WT cells (inner circle) and 7875 Prmt1 KO cells (outer circle). Eight transcriptionally distinct clusters were identified (clusters 1–8 of indicated colors) by unsupervised classification. (**E**) The bubble chart showed that cluster 1 was marked by upregulated expression of PrE marker genes and cluster 2 was marked by upregulated 2C-like genes. (**F**) RNA velocity of scRNA-seq showed the transcription rate (arrows).

of PrE cells (Figure 1F). These results indicated that Prmt1 depletion led to the emergence of a cell population with features of progenitors of PrE within mESCs.

Prmt1 reduces the potential of ESCs differentiated toward XEN cells

XEN cells represent an *in vitro* variant of stem cells representative of the extraembryonic endoderm fate (48,49). A chemical induction of XEN cells was performed as previously (36). Fluorescence-activated cell sorting (FACS) assay showed that *Prmt1* KO cells had higher efficiency of XEN induction than WT cells (Figure 2A), which indicated that Prmt1 depletion made the ESCs prone to XEN cells. Interestingly, without induction, approximately one percent of the *Prmt1* KO cells showed XEN features, as represented by high expression of Gata6 and low expression of Nanog ($Gata6^+/Nanog^-$). This ratio is consistent with the number of cells within cluster 1 in the scRNA-Seq data (Figure 1D). Furthermore, after XEN induction, >30% of the *Prmt1* KO cells acquired features of XEN cells, while only 1.55% of WT cells successfully became XEN cells (Figure 2A). These results suggested that Prmt1 acts as a safe-guarder of ESCs preventing from differentiation to XEN cells.

To ascertain the role of Prmt1 in XEN induction, Prmt1 was rescued in *Prmt1* KO cells by re-expressing Prmt1 and its catalytically inactive mutant E153Q (Prmt1m) (50). Re-expression of Prmt1, but not Prmt1m, in *Prmt1* KO cells clearly reduced the proportion of $Gata6^+/Nanog^-$ cells (6.54% versus 30.8%) (Figure 2B). The results confirmed that Prmt1, especially *via* its enzymatic function, decreased the differentiation potential of ESCs to XEN fate. Furthermore, the Prmt1-specific inhibitor, furamidine dihydrochloride (Fur) (51), was employed to treat the E14 cells. By using novel generated anti-Klf4Rme2a, western blot showed that Fur treatment could reduce the level of methylation of Klf4 in ES cells (Figure 2C). FACS assays showed that Fur treatment obviously increased the $Gata6^+/Nanog^-$ cell proportion both with and without chemical induction in a dose-dependent manner (Figure 2D). Moreover, IF assays showed that Fur treatment increased the number of $Gata6^+/Nanog^-$ cells among XEN-inducing cells (Figure 2E). Taken together, we demonstrate that Prmt1 could prevent spontaneous differentiation of ESCs to XEN cells.

Klf4 is involved in Prmt1-mediated chromatin remodeling on PrE genes

To gain insight into the mechanism by which Prmt1 regulates PrE genes related to the emergence of XEN cells, DNase I sensitivity assays were performed as previously described (39) to investigate whether Prmt1 could affect chromatin accessibility at the promoters of PrE genes. The results showed that Prmt1 depletion made the chromatin of PrE genes, including the *Gata4* and *Gata6* genes, more accessible at the promoter regions (Figure 3A). ChIP-qPCR assays revealed that the enrichments of histone acetylation of H3 and H4 (H3ac and H4ac) in the promoters

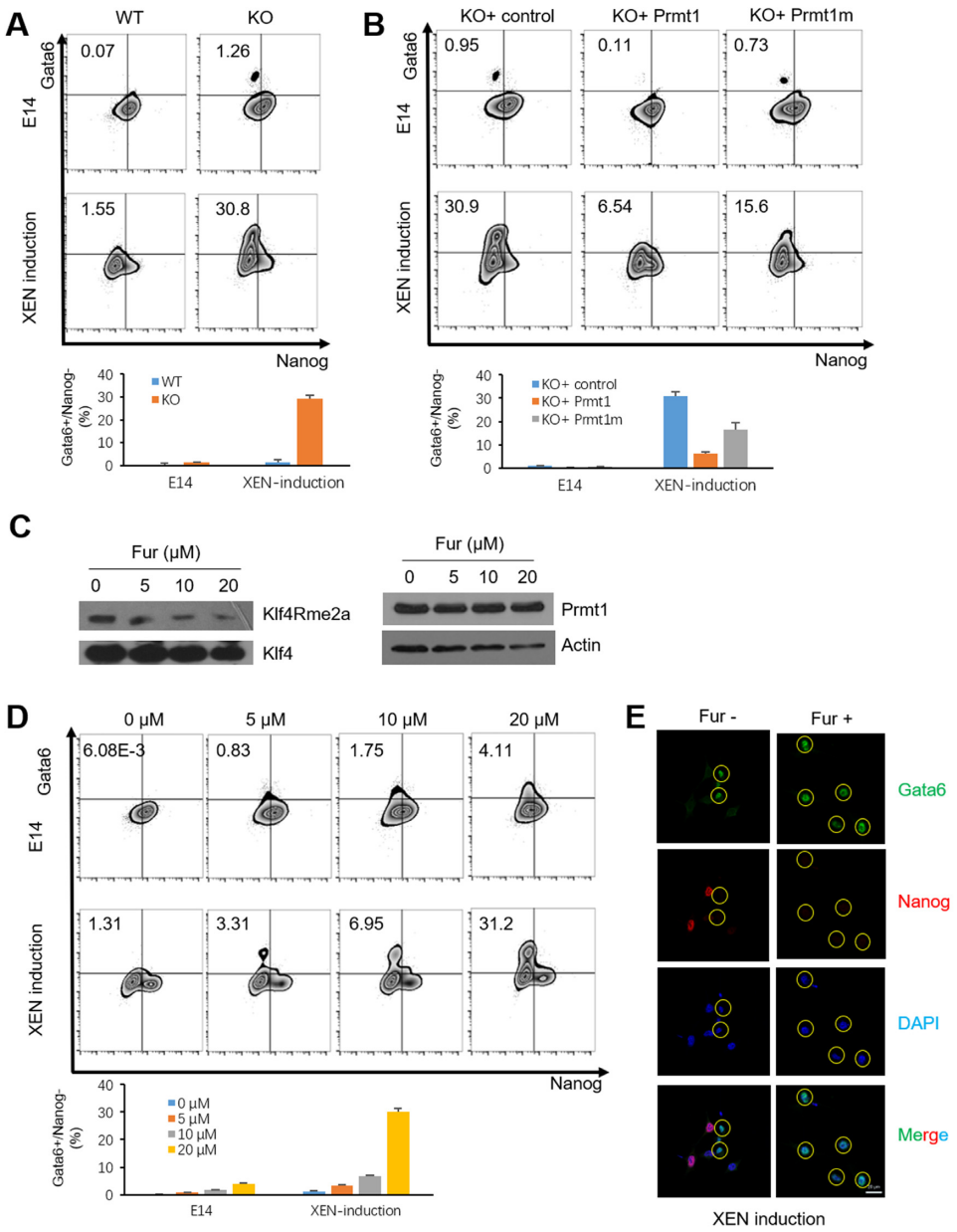

Figure 2. Prmt1 depletion accelerates XEN induction in mouse ESCs. (**A**) FACS was performed by labelling Gata6 and Nanog in mouse ESCs without or with XEN induction (upper panels). The percentage of Gata6+/Nanog– cells is shown in the lower panel. (**B**) FACS showed the impact of Prmt1 rescue in its KO cells. Based on the Prmt1 KO background, a Prmt1 rescue (Prmt1) and an enzyme-inactive (Prmt1m) cell lines were generated and used for XEN induction (upper panels). The percentage of Gata6+/Nanog– cells is shown in the lower panel. (**C**) The effect of Fur treatment on E14 cells. (**D**) FACS showed the impact of an inhibitor of Prmt1 (Fur) in E14 cells with and without XEN induction (upper panels). The percentage of Gata6+/Nanog- cells is shown in the lower panel. (**E**) IF assays showed the impact of Fur on the expression of Gata6 (green) and Nanog (red) in E14 cells with XEN induction. Nuclei were visualized with DAPI staining (blue). Yellow circles indicate Gata6+ cells.

of the *Gata4* and *Gata6* genes were dramatically increased in *Prmt1* KO cells, while other modifications (repressive H3K9me2, K3K9me3, H3K27me3 and active H3K4me3) were not changed (Figure 3B). It must be mentioned that the levels of H4R3me2 on the *Gata4* and *Gata6* genes were low in WT cells and did not change in *Prmt*1 KO cells, although the global levels of this modification decreased in Prmt1 KO cells (middle panels, Supplementary Figure S1B), which implied that the decrease in H4R3me2 might make a little contribution to the activation of PrE genes. In addition, hyperacetylation of H3 and H4 mediated by Prmt1 depletion was observed in the promoters of *Sox17*, *Sox7*, *Pdgfra* and *Amn* (Supplementary Figure S4). These results indicated that altered histone acetylation rather than histone arginine (or lysine) methylation could be the cause of chromatin changes at PrE gene after Prmt1 depletion. Furthermore, ChIP-qPCR assays were performed by using antibodies specific for the mSin3a complex (HDAC1, HDAC2, and mSin3a) and the heterochromatic complex (HP1). The results showed that HDAC1, HDAC2 and mSin3a, but not

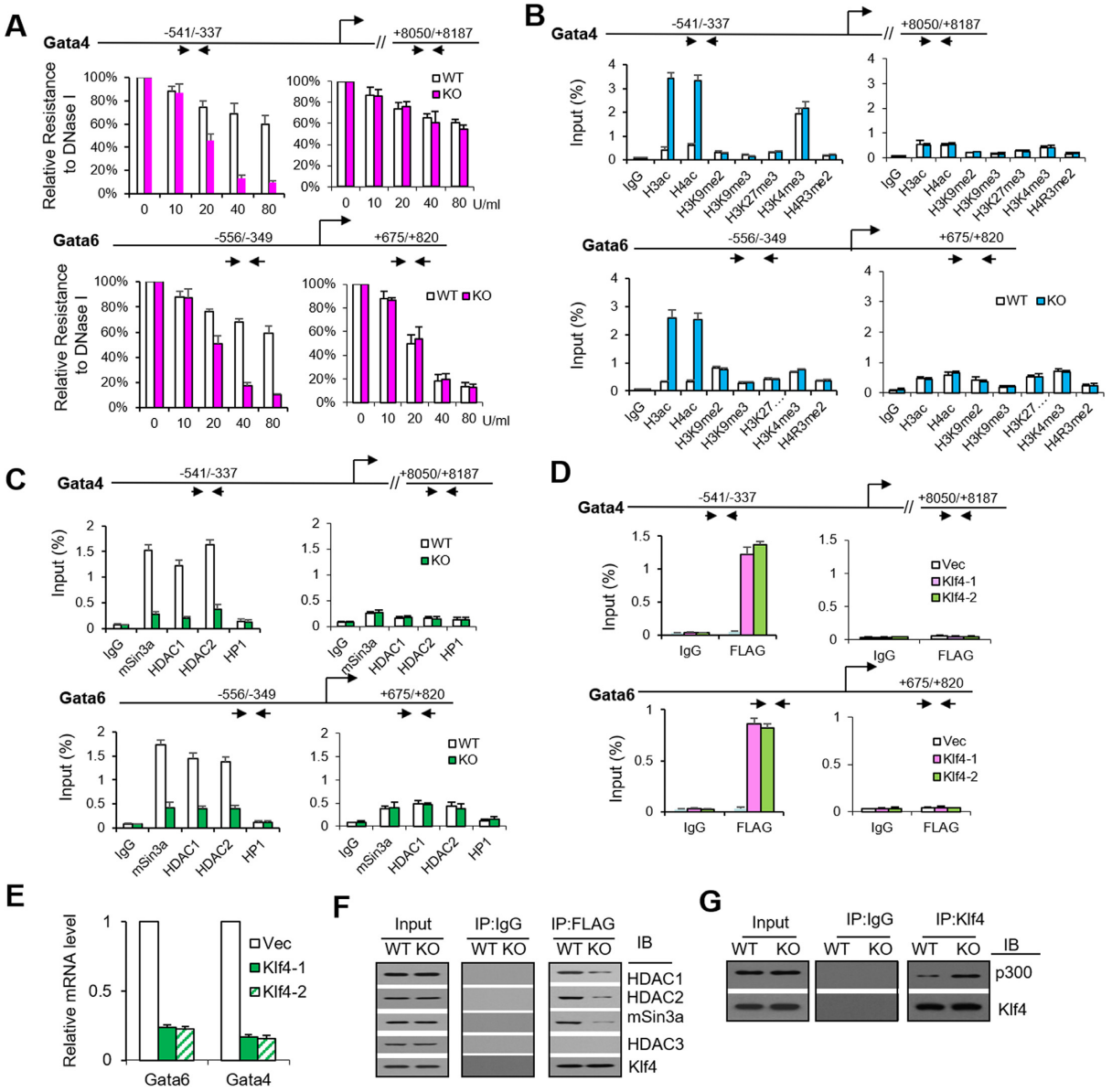

Figure 3. Klf4 is involved in chromatin remodeling of PrE genes mediated by Prmt1. (**A**) DNase I sensitivity analysis showed open chromatin in the promoter regions of the Gata4 and Gata6 genes in WT (open bars) and Prmt1 KO (filled bars) cells. The indicated amounts of DNase I (0, 10, 20, 40 and 80 U/ml) were used. (**B** and **C**) ChIP-qPCR analysis of the occupancy of histone modifications (H3ac, H4ac, H3K9me3, H3K27me3, H3K4me3 and H4R3me2) (B) and the repressive complex (mSin3a, HDAC1, HDAC2, and HP1) (C) in the upstream region of Gata4 and Gata6 in WT (open bars) and Prmt1 KO (filled bars) cells. Regions +8050 of Gata4 and +733 of Gata6 were used as negative control regions for the genes. An anti-FLAG antibody was used for ChIP. IgG was used as a ChIP control. (**D**) ChIP-qPCR analysis of ectopic FLAG-Klf4 binding to the promoters of Gata4 and Gata6 in E14 cells. (**E**) RT-qPCR showed the effect of ectopic Klf4 on the expression of the Gata4 and Gata6 genes. Empty vector was transfected into E14 cells as a control (Vec). (**F**) Co-IP assays of Klf4 with the mSin3a complex in E14 cells. Whole-cell extracts (WCEs) of WT and Prmt1 KO cells were subjected to IP with an anti-Klf4 antibody and then blotted with antibodies specific for HDAC1, HDAC2, mSin3a, Klf4 and HDAC3 as a negative control. WCEs that were not subjected to IP were used as the input. IgG was used as a negative control. (**G**) Co-IP assays of Klf4 with p300 in E14 ES cells.

HP1, were recruited to the promoters of the *Gata4* and *Gata6* genes (open bars, Figure 3C). The recruitment of the mSin3a complex was significantly reduced in Prmt1 KO cells (filled bars, Figure 3C) for further activation of the *Gata4* and *Gata6* genes.

Interestingly, the promoter regions of PrE genes described above contain putative Klf4-binding sites (CACCC), including the –541/–337 bp region for *Gata4* (–340 bp) and –556/–349 bp for *Gata6* (–496 bp). Klf4 belongs to the Krüppel-like family (KLF) proteins, which have been reported to be involved in pluripotency maintenance and mouse embryonic development (52–55). To address the mechanistic role of Klf4 in Prmt1-mediated gene expression, stable E14 cell lines with ectopic expression of Klf4 were generated by infection with lentiviral vectors expressing FLAG-Klf4 (designated Klf4-1 and Klf4-2), with a GFP lentiviral vector as a control. ChIP-qPCR assays showed that ectopic Klf4 occupied the putative

Klf4-binding sites in the promoter of the PrE genes *Gata4* (–340 bp) and *Gata6* (–496 bp) (Figure 3D). Meanwhile, RT-qPCR assays showed that the mRNA levels of *Gata4* and *Gata6* were reduced by ectopic Klf4 (Figure 3E). Co-IP assays showed that the interaction between Klf4 and the mSin3a complex was weaker in Prmt1 KO cells (Figure 3F). Furthermore, the binding of p300 to Klf4 was obviously increased (Figure 3G). Taken together, our data suggest that Klf4 occupancy at PrE gene promoters is involved in the inhibition of PrE genes *via* the mSin3a complex and that depletion of Prmt1 could alleviate this repression and lead to the activation of PrE genes in mESCs.

Klf4 methylated by Prmt1 at R396 is required for repression of PrE genes

Considering that both Prmt1 and Klf4 are involved in PrE gene expression, we hypothesized that Prmt1 might methylate Klf4 directly and affect its regulatory functions. To confirm this hypothesis, we examined the interaction between Prmt1 and Klf4. Co-IP and GST pulldown assays showed an interaction between Prmt1 and Klf4 (Figure 4A and B). To identify the binding region of Klf4 that was responsible for the interaction, FLAG-tagged truncations of Klf4 were constructed. Pulldown assays using GST-Prmt1 indicated that the 401–483 aa region of Klf4 is responsible for its association with Prmt1 (Figure 4C). Reverse GST pulldown assays for FLAG-Prmt1 confirmed that the fragment from 401 to 483 aa of Klf4 bound to Prmt1; moreover, the region from 386 to 400 aa impeded the interaction between them (Figure 4D). Next, *in vitro* methylation assays showed that full-length Klf4 (1-483 aa) was methylated in the presence of Prmt1 but not Prmt1m (Prmt1 E153Q mutation) (lane 3 versus lane 4, Figure 4E). Notably, ^{3}H signals were also observed on the 386–400 aa and 1–400 aa fragments but not on other derivatives (lanes 9 and 11, Figure 4E), which indicated that the arginine methylation site should be located between 386 and 400 aa in Klf4. Furthermore, an *in vitro* methylation assay followed by mass spectrometric (MS) analysis indicated that arginine residue R396 was di-methylated by Prmt1 (Figure 4F). No ^{3}H signal was detected in the methylation assay when arginine 396 of Klf4 was mutated to lysine (R396K) (Figure 4G), which confirmed that R396 of Klf4 was methylated by Prmt1.

To certify the endogenous Klf4 is methylated at R396, a specific antibody against asymmetric di-methylated R396 of Klf4 (Klf4Rme2a) was generated, western blot using anti-Klf4Rme2a showed that Klf4 was methylated in the ES cells while the methylated signal was obviously decreased in Prmt1 KO cells (Figure 4H). Most importantly, when R396 of Klf4 was mutated *in situ* to alanine (R396A) in AB2.2 ES cells, the endogenous signal of arginine methylated Klf4 was significantly reduced (Figure 4I).

To investigate the role of arginine-methylated Klf4, R396 mutations were used to examine the effect of Klf4 on PrE genes. RT-qPCR assays showed that the R396A or R396K mutation of Klf4 was no longer able to suppress the expression of *Gata4* and *Gata6*, similar with that of WT Klf4 (Figure 4K). ChIP-qPCR data showed that the mSin3a complex (mSin3a, HDAC1 and HDAC2) was no longer recruited to the promoters of the *Gata4* and *Gata6* when R396 of Klf4 was mutated (R/K or R/A), even though these mutants still occupied the promoters themselves (Figure 4L). These results indicated that the R396 mutation of Klf4 could not repress the PrE genes due to failed recruitment of the mSin3a complex. Co-IP assays of ectopic Klf4 or its mutants in E14 cells showed that R396 mutations of Klf4 (R/K and R/A) impeded the interaction of Klf4 with the mSin3a complex (Figure 4M). Furthermore, pull down assay using peptide of Klf4 containing R396 showed that arginine methylated peptide could specifically bind to HDAC1 in vitro, while unmethylated one could not (Figure 4J). Intriguingly, ChIP/re-ChIP assays confirmed that Klf4 co-occupied the promoter of Gata6 with the mSin3a complex, while the R/K mutant did not (Figure 4N). These results indicated that R396 of Klf4 is crucial for interaction with and recruitment of the mSin3a complex at the promoter regions of PrE genes.

To examine whether arginine methylation of Klf4 contributed to the induction of XEN cells, FACS assays showed that ectopic Klf4 markedly inhibited the XEN induction, the R396A mutant, an unmethylated form, reduced the inhibitory effects to some extent (Figure 4O). The result suggested that Klf4 methylation might be involved in preventing the emergence of PrE progenitors from mESCs.

Prmt1 regulates the PrE commitment *in vivo*

To investigate the function of Prmt1 in mouse embryo development, Fur was employed to treat mouse AB2.2 ES cells stably expressed GFP and td-Tomato (37). Then the treated cells were injected into the mouse E3.5 blastocyst. E6.5 chimeric embryos were dissected and observed with a fluorescence stereomicroscope (FSM) and confocal laser stereomicroscope (CLSM) (Figure 5A). We found that without Fur treatment (Fur–), the injected GFP^{+}/td-Tomato^{+} cells mainly integrated into Epiblast (EPI) showing in the yellow inter-continuous circles, Fur treatment (Fur+) made the cells integrated into both EPI and PrE (outside of the circle) (Figure 5B). Further observations of chimeric embryos at E12.5 and mice after birth showed that the Fur-treated cells were still capable of integration (Supplementary Figure S5). The results suggested that Prmt1 is likely to participate in the second cell fate decision during mouse embryo development, potentially by restricting the PrE commitment. To confirm the function of Prmt1 in early embryogenesis, mouse blastocysts were treated with Fur. IF images showed that Gata6 was induced, while the level of Nanog was reduced by Fur treatment in mouse blastocysts (Figure 5C). Inhibition of Prmt1 significantly increased the percentage of Gata6-positive cells (Figure 5D). Furthermore, IF showed that Fur treatment induced Gata6 gene expression while reducing the expression of Nanog in cultured E14 cells (Figure 5E). Moreover, RT-qPCR showed that inhibition of Prmt1 induced the expression of the *Gata4* and *Gata6* genes at the mRNA level (Figure 5F). Our data indicate that inhibition of Prmt1 can induce the expression of Gata6 to bias the fate of pluripotent cells toward the PrE lineage.

To confirm the effect of methylation of Klf4 at R396 on the PrE commitment *in vivo*, AB2.2 ES cells containing R396A mutation *in situ* were employed to be microinjected into mouse E3.5 blastocysts. The chimeric embryos

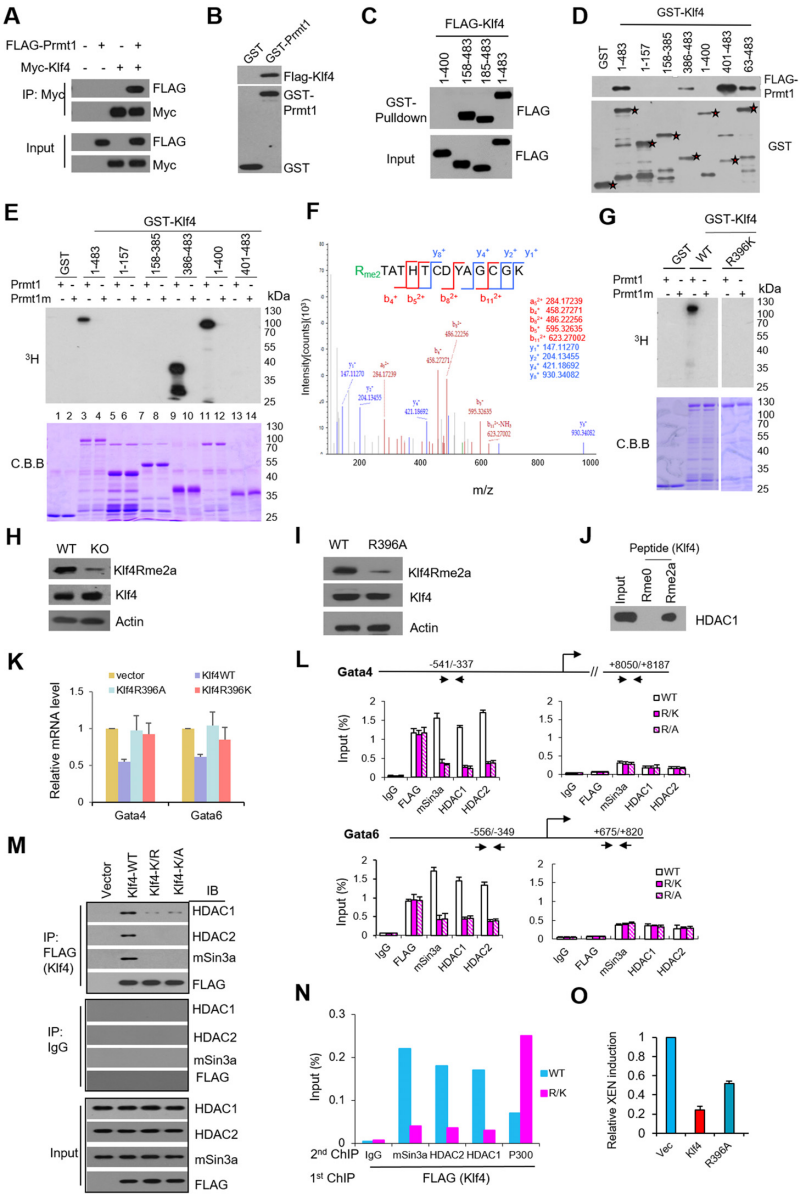

Figure 4. Klf4 methylated by Prmt1 at R396 is involved in the expression of PrE genes. (**A**) Co-IP of Prmt1 and Klf4. Whole-cell extracts (WCEs) of HEK293T cells transfected with (+) or without (–) Myc-Klf4 and/or FLAG-Prmt1 were subjected to IP with an anti-Myc antibody and blotted with antibodies specific for FLAG for Prmt1 and Myc for Klf4. (**B**) GST pulldown assays to detect the interaction of Prmt1 with Klf4. GST or GST-Prmt1 was incubated with WCEs of HEK293T cells expressing FLAG-Klf4 and then blotted with antibodies specific for FLAG or GST. (**C**) Purified GST-Prmt1 was incubated with WCEs of HEK293T cells expressing FLAG-Klf4 and its truncations. The GST pulldown products were immunoblotted with an anti-FLAG antibody, and WCEs that were not subjected to IP were used as the input. (**D**) Purified GST-Klf4 and its derivatives were incubated with WCEs of HEK293T cells expressing FLAG-Prmt1 or vector. The GST pulldown products were then immunoblotted with an anti-FLAG antibody for Prmt1 or an anti-GST antibody. (**E**) Autoradiography of in vitro methylation assays using purified GST-Klf4 and its derivatives with Prmt1 or Prmt1m (an inactive enzymatic mutant). Total amounts of GST-Klf4 and Klf4 truncations were visualized by Coomassie brilliant blue (C.B.B.) staining. (**F**) MS analysis of a Klf4 peptide mixture to identify methylated sites *in vitro*. Dimethylated arginine (Rme2) is displayed in green. (**G**) Autoradiography of in vitro methylation assays using purified GST-Klf4 and an R396K mutant of Klf4 with Prmt1 or Prmt1m. (**H**) Western blotting assay with anti-Klf4R396me2a, Klf4, and Actin in E14 ES cells (WT) and Prmt1 KO cells. (**I**) Western blotting assay with anti-Klf4R396me2a, Klf4, and Actin in AB2.2 ES cells without (WT) or with R396A mutation of Klf4 (R396A). (**J**) Peptide pulldown assay with purified HDAC1 by unmethylated peptide of Klf4 (Rme0) or asymmetric di-methylated peptide of Klf4 (Rme2a). (**K**) RT-qPCR analysis showed the effects of Klf4-WT, Klf4-R396A, Klf4-R396K and vector on the expression levels of Gata4 and Gata6 in E14 cells. (**L**) ChIP assays showed the recruitment of mSin3a, HDAC1, and HDAC2 to the promoters of Gata4 and Gata6 in E14 cells transfected with Klf4 (WT) or Klf4 point mutants at R396 (R/K or R/A). (**M**) Co-IP assays of Klf4 with the mSin3a complex. WCEs of E14 cells transfected with FLAG-Klf4 (WT) or its R396 mutants (Klf4-R/K or Klf4 R/A) were subjected to IP with an anti-FLAG antibody and then blotted with antibodies specific for HDAC1, HDAC2, mSin3a and FLAG for Klf4. WCEs that were not subjected to IP were used as the input. IgG was used as a negative control. (**N**) ChIP/re-ChIP assays showed that Klf4-mediated mSin3a/HDAC recruitment to the promoter of Gata6 is arginine methylation dependent. E14 cells were transfected with FLAG-Klf4 (WT) or its mutant at R396 (R/K). An anti-FLAG antibody was used for the initial ChIP (first) to obtain the Klf4-associated chromatin fragments. Then, these fragments were subjected to re-ChIP (second) using mSin3a, HDAC1, and HDAC2 antibodies. IgG was used as a ChIP control. (**O**) FACS showed the impact of mutant R396 of Klf4 in E14 cells transfected with Klf4 and its mutants R396A and R396F. The percentage of $Gata6^{+}/Nanog^{-}$ cells is shown.

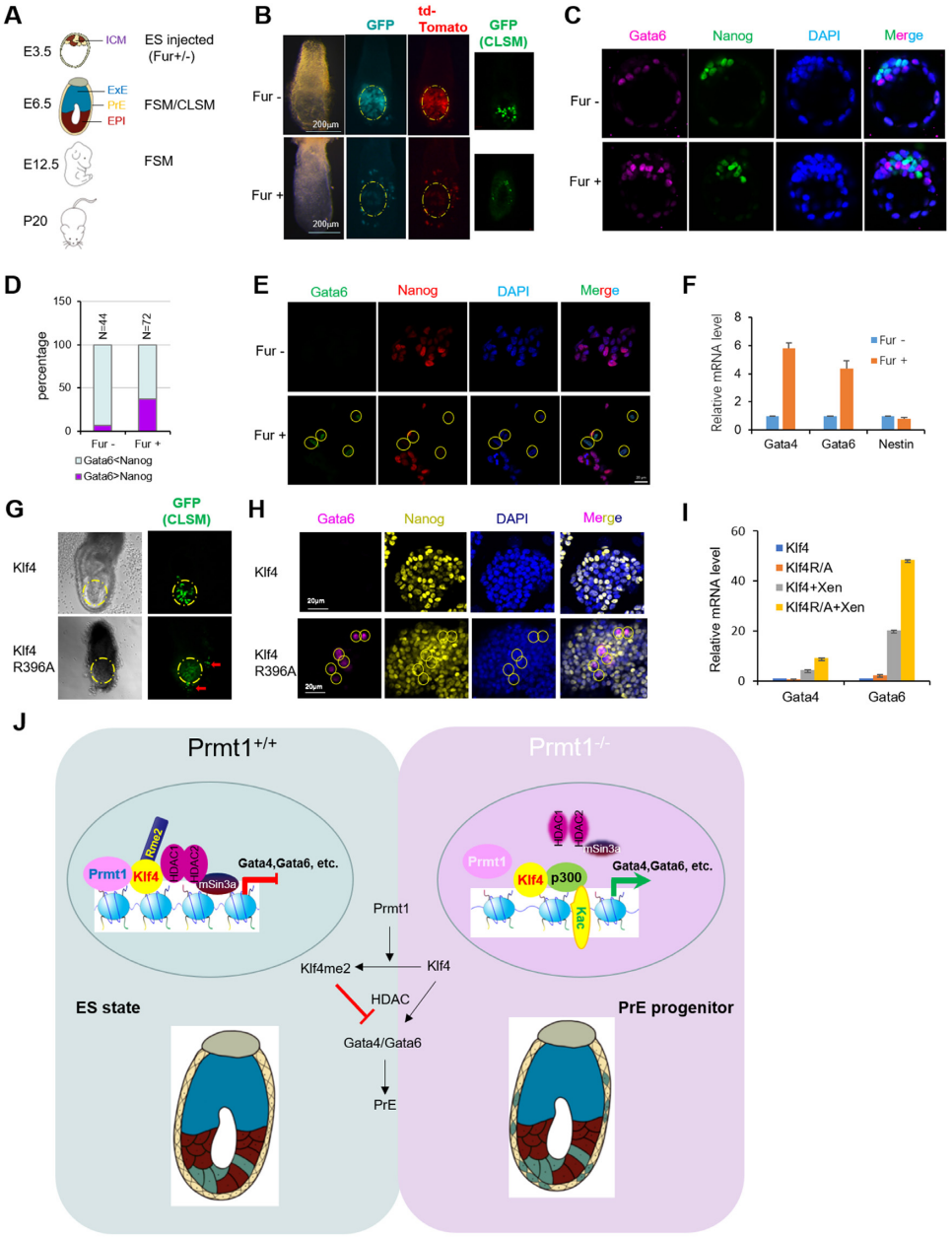

Figure 5. The effects of Prmt1 inhibition and R396A mutant of Klf4 on the PrE commitment. (**A**) Scheme of the chimeric assay. (**B**) Chimeric assay of ES cells with (Fur+) or without (Fur–) treatment. The ES cell line was AB2.2 cells with GFP and td-Tomato. After Fur treatment for 24 h, cells were microinjected into blastocysts. Embryos were observed at E6.5. GFP (green) and Td-Tomato (red) signals were detected. Dashed lines mark epiblasts. (**C**) IF assays showed the effect of Fur on mouse blastocysts. Blastocysts were cultured with (Fur+) or without (Fur–) for 24 h and then immunostained with Gata6 (red) to indicate PrE and Nanog (green) to indicate EPI. (**D**) Distribution of two cell types in the ICM. (**E**) IF assays showed the impact of Fur on the expression of Gata6 (green) and Nanog (red) in E14 cells with XEN induction. Nuclei were visualized with DAPI staining (blue). Yellow circles indicate Gata6-positive cells. (**F**) Fur treatment induced the expression of Gata4 and Gata6 genes using RT-qPCR, and Nestin was used as a negative control. (**G**) Chimeric assay of ES cells of wild type Klf4 and mutant Klf4 R396A. The AB2.2 cells were microjnjected into blastocysts. Embryos were observed at E6.5. Dashed yellow lines marked epiblasts, the arrows indicated chimeric cells outside of epiblasts. (**H**) IF assays showed the impact of Klf4 R396A mutation in AB2.2 cells. Nuclei were visualized with DAPI staining (blue). Yellow circles indicate Gata6-positive cells. (**I**) RT-qPCR assay showed that XEN induction further increased the expression of Gata4 and gata6 genes in R396A mutation in AB2.2 ES cells. (**J**) Schematic depiction of Klf4 methylation by Prmt1 to regulate PrE gene expression *via* mSin3a/HDAC recruitment in mouse ESCs, which heterogeneously prevents a bias toward PrE commitment.

at E6.5 were dissected and observed with confocal laser stereomicroscope (CLSM) and the results were shown that Klf4R396A mutant could integrate into PrE regions (red arrows outside of the yellow circles) compared with AB2.2 cells with wild type Klf4 (Figure 5G). Similar with Fur treatment, IF assays showed that Gata6 increased in AB2.2 cells with R396A mutation of Klf4 (Figure 5H). RT-qPCR analysis showed that XEN induction could further enhance the expression of Gata4 and Gata6 genes in AB2.2 cells with R396A mutation of Klf4 (Figure 5I).

Taken together, the data suggested that the methylation of Klf4 at R396 by Prmt1 should reduce the expression of PrE genes in ES cells and might restrain the PrE commitment in mouse blastocysts.

DISCUSSION

Arginine methylation has emerged as a prevalent posttranslational modification involved in diverse biological processes (23,24,56). Prmt1 can regulate many important processes via methylation of its histone and nonhistone substrates. The importance of Prmt1 in mouse embryo development has long been known, as Prmt1 knockout leads to early embryo lethality. However, the underlying molecular mechanisms for lethality remain unclear. In this report, we used mouse ES cells as a tool to illustrate the functions of Prmt1 in ES cell fate control. Prmt1 depletion leads to the emergence of a small population of XEN cells within ES cells, as determined using immunostaining and scRNA-Seq. Depletion of Prmt1 increases acetylation of histone H3 and H4 and leads to an open chromatin state at PrE genes. Based on careful biochemical and molecular mechanistic characterization, we suggest that Prmt1 methylates Klf4, the methylation state of which affects its binding and recruitment of the HDAC complex at PrE gene promoters for PrE gene expression. *In vivo* experiments further indicated that Prmt1 could regulate PrE lineage commitment (Figure 5I).

Posttranslational modification has long been believed to be a rapid and finely tuned method of gene regulation, especially for developmental processes (23). Pax7 methylation mediated by Prmt1 has been reported to regulate the muscle development (57). The zygotic genome needs time for reactivation after fertilization, and precise activation of genes may depend on more finely tuned switches. Little is known regarding posttranslational regulation during early embryo development. Our results proved that Klf4 methylation mediated by Prmt1 may act as a regulatory factor as early as the early blastomere stage.

Regulation of preimplantation embryo development is a fundamental biological question. Due to the short time window of preimplantation and rareness of blastomere samples, mESCs are used as a tool to understand the regulatory pathways involved in mouse preimplantation development. It remains challenging to extend conclusions from ESCs into normal embryo development. The second cell fate decision, in other words, how ICM cells differentiate into PrE and EPI cells, has been an active research topic for many years. It is well known that in the ICM, a 'salt and pepper' expression pattern arises at E3.5 (8,11). That is, some ICM cells display increased expression of *Gata4* and *Gata6*, but decreased expression of Nanog leads to the formation of the PrE layer, while the EPI fate is acquired in cells with high Nanog. How these two portions of cells are selected remains largely unclear. The segregation of the EPI and PrE lineages in the ICM is regulated by fibroblast growth factor (FGF) signaling (58). Fgf4, FGF receptor 2 (Fgfr2) and Grb2, which together mediate activation of the mitogen-activated protein kinase signalling pathway, are necessary for PrE formation. Our data revealed that arginine methylation of Klf4 by Prmt1 regulated the appearance of XEN cells, which provides a novel epigenetic mechanism for the second cell fate decision in mouse embryogenesis. Our results indicated that Prmt1 regulated the expression of PrE genes to bias the cell fate toward XEN cells, which could result in unbalanced cell numbers between EPI and PrE cells. These unbalanced proportions of ICM stem cells may explain why Prmt1$^{-/-}$ mice died around the implantation of blastocysts with normal extraembryonic tissues (34). Carm1 functions in directing the initial stem cell fate *via* heterogeneous regulation of the Oct4 and Sox2 target genes (27). Interestingly, our data indicated that Prmt1 might participate in the second cell fate decision in early embryo development by regulating the PrE lineage.

In addition to transcriptional activation *via* methylation of histone H4R3 (59,60), Prmt1 participates in transcriptional regulation *via* nonhistone targets, such as Foxo1, Runx1 and C/EBPα (61–63). Our data revealed that heterogeneity in the expression of PrE genes regulated by Prmt1 depends on Klf4 methylation rather than H4R3me, revealing a novel nonhistone target of Prmt1. An increasing number of studies have revealed crucial roles of the KLF in embryonic development (54). Among the 18 members of the KLF, only Klf4 and Klf5 are expressed as early as the two-cell stage, with persistent expression until blastocyst formation (55,64–66), indicating their significance and similar functions. During the process of Prmt1-mediated regulation of the expression of PrE genes, Klf4 is a mediator that depends on its R396 methylation status, which gives us new insights into the role of Klf4 in ES cells and embryonic development. Notably, symmetric arginine methylation of Klf4 by Prmt5 was reported to inhibit Klf4 turnover in breast carcinogenesis (67), suggesting the function of Klf4 methylation.

Combined with the scRNA-seq data, our experiments provide a microscopic view of the gene regulation process at the single-cell level. Approximately 1% of ES cells show obvious XEN features after Prmt1 knockout. This percentage can be regarded as a link between the result obtained with traditional large-scale molecular methods and microscopic single-cell data. Either Prmt1 knockout or Prmt1 inhibitor treatment predisposes mouse ES cells to XEN cell development, which should contribute to the efficient production of XEN cell lines from mouse ES cells, which are useful cell culture models of the PrE lineage (36,48,68). During chemical reprogramming, the formation of XEN-like cells marked by Gata4, Gata6 and Sox17 helps to generate iPSCs with high efficiency (69,70). Our data might offer new possibilities for chemical reprogramming by targeting the Prmt1/Klf4 regulatory pathway.

SUPPLEMENTARY DATA

Supplementary Data are available at NAR Online.

ACKNOWLEDGEMENTS

We thank Dr Pedro Rocha of NIH for critical reading of manuscript.We thank NovelBio Bio-Pharm Technology Co.,Ltd for the support of scRNA-seq experiment and bioinformatics analysis By NovelBrain Cloud.

FUNDING

CAMS Innovation Fund for Medical Sciences [2016-I2M-3-002 to Y.Z. and Y.H., 2017-I2M-3-009 to M.C. and H.D., 2021-I2M-1-019 to Y.H.]; National Natural Science Foundation of China [91519301 to Y.Z., 31871310 to Y.Z., 31970813 to Y.H]. Funding for open access charge: Chinese Academy of Medical Sciences.

Conflict of interest statement. None declared.

REFERENCES

1. Shahbazi,M.N. and Zernicka-Goetz,M. (2018) Deconstructing and reconstructing the mouse and human early embryo. *Nat. Cell Biol.*, **20**, 878–887.
2. Zernicka-Goetz,M., Morris,S.A. and Bruce,A.W. (2009) Making a firm decision: multifaceted regulation of cell fate in the early mouse embryo. *Nat. Rev. Genet.*, **10**, 467–477.
3. Saiz,N. and Plusa,B. (2013) Early cell fate decisions in the mouse embryo. *Reproduction (Cambridge, England)*, **145**, R65–80.
4. Johnson,M.H. and Ziomek,C.A. (1981) The foundation of two distinct cell lineages within the mouse morula. *Cell*, **24**, 71–80.
5. Strumpf,D., Mao,C.A., Yamanaka,Y., Ralston,A., Chawengsaksophak,K., Beck,F. and Rossant,J. (2005) Cdx2 is required for correct cell fate specification and differentiation of trophectoderm in the mouse blastocyst. *Development (Cambridge, England)*, **132**, 2093–2102.
6. Niwa,H., Toyooka,Y., Shimosato,D., Strumpf,D., Takahashi,K., Yagi,R. and Rossant,J. (2005) Interaction between Oct3/4 and Cdx2 determines trophectoderm differentiation. *Cell*, **123**, 917–929.
7. Nichols,J., Zevnik,B., Anastassiadis,K., Niwa,H., Klewe-Nebenius,D., Chambers,I., Scholer,H. and Smith,A. (1998) Formation of pluripotent stem cells in the mammalian embryo depends on the POU transcription factor Oct4. *Cell*, **95**, 379–391.
8. Chazaud,C., Yamanaka,Y., Pawson,T. and Rossant,J. (2006) Early lineage segregation between epiblast and primitive endoderm in mouse blastocysts through the Grb2-MAPK pathway. *Dev. Cell*, **10**, 615–624.
9. Xenopoulos,P., Kang,M., Puliafito,A., Di Talia,S. and Hadjantonakis,A.K. (2015) Heterogeneities in Nanog expression drive stable commitment to pluripotency in the mouse blastocyst. *Cell Rep.*, **10**, 1508–1520.
10. Guo,G., Huss,M., Tong,G.Q., Wang,C., Li Sun,L., Clarke,N.D. and Robson,P. (2010) Resolution of cell fate decisions revealed by single-cell gene expression analysis from zygote to blastocyst. *Dev. Cell*, **18**, 675–685.
11. Plusa,B., Piliszek,A., Frankenberg,S., Artus,J. and Hadjantonakis,A.K. (2008) Distinct sequential cell behaviours direct primitive endoderm formation in the mouse blastocyst. *Development (Cambridge, England)*, **135**, 3081–3091.
12. Nakai-Futatsugi,Y. and Niwa,H. (2015) Epiblast and primitive endoderm differentiation: fragile specification ensures stable commitment. *Cell Stem. Cell*, **16**, 346–347.
13. Mitsui,K., Tokuzawa,Y., Itoh,H., Segawa,K., Murakami,M., Takahashi,K., Maruyama,M., Maeda,M. and Yamanaka,S. (2003) The homeoprotein Nanog is required for maintenance of pluripotency in mouse epiblast and ES cells. *Cell*, **113**, 631–642.
14. Frankenberg,S., Gerbe,F., Bessonnard,S., Belville,C., Pouchin,P., Bardot,O. and Chazaud,C. (2011) Primitive endoderm differentiates via a three-step mechanism involving Nanog and RTK signaling. *Dev. Cell*, **21**, 1005–1013.
15. Schrode,N., Saiz,N., Di Talia,S. and Hadjantonakis,A.K. (2014) GATA6 levels modulate primitive endoderm cell fate choice and timing in the mouse blastocyst. *Dev. Cell*, **29**, 454–467.
16. Fujikura,J., Yamato,E., Yonemura,S., Hosoda,K., Masui,S., Nakao,K., Miyazaki Ji,J. and Niwa,H. (2002) Differentiation of embryonic stem cells is induced by GATA factors. *Genes Dev.*, **16**, 784–789.
17. Koutsourakis,M., Langeveld,A., Patient,R., Beddington,R. and Grosveld,F. (1999) The transcription factor GATA6 is essential for early extraembryonic development. *Development (Cambridge, England)*, **126**, 723–732.
18. Niakan,K.K., Ji,H., Maehr,R., Vokes,S.A., Rodolfa,K.T., Sherwood,R.I., Yamaki,M., Dimos,J.T., Chen,A.E., Melton,D.A. *et al.* (2010) Sox17 promotes differentiation in mouse embryonic stem cells by directly regulating extraembryonic gene expression and indirectly antagonizing self-renewal. *Genes Dev.*, **24**, 312–326.
19. Soudais,C., Bielinska,M., Heikinheimo,M., MacArthur,C.A., Narita,N., Saffitz,J.E., Simon,M.C., Leiden,J.M. and Wilson,D.B. (1995) Targeted mutagenesis of the transcription factor GATA-4 gene in mouse embryonic stem cells disrupts visceral endoderm differentiation in vitro. *Development (Cambridge, England)*, **121**, 3877–3888.
20. Artus,J., Piliszek,A. and Hadjantonakis,A.K. (2011) The primitive endoderm lineage of the mouse blastocyst: sequential transcription factor activation and regulation of differentiation by Sox17. *Dev. Biol.*, **350**, 393–404.
21. Atlasi,Y. and Stunnenberg,H.G. (2017) The interplay of epigenetic marks during stem cell differentiation and development. *Nat. Rev. Genet.*, **18**, 643–658.
22. Jambhekar,A., Dhall,A. and Shi,Y. (2019) Roles and regulation of histone methylation in animal development. *Nat. Rev. Mol. Cell Biol.*, **20**, 625–641.
23. Blanc,R.S. and Richard,S. (2017) Arginine methylation: the coming of age. *Mol. Cell*, **65**, 8–24.
24. Guccione,E. and Richard,S. (2019) The regulation, functions and clinical relevance of arginine methylation. *Nat. Rev. Mol. Cell Biol.*, **20**, 642–657.
25. Vougiouklakis,T., Nakamura,Y. and Saloura,V. (2017) Critical roles of protein methyltransferases and demethylases in the regulation of embryonic stem cell fate. *Epigenetics*, **12**, 1015–1027.
26. Yang,Y. and Bedford,M.T. (2013) Protein arginine methyltransferases and cancer. *Nat. Rev. Cancer*, **13**, 37–50.
27. Goolam,M., Scialdone,A., Graham,S.J.L., Macaulay,I.C., Jedrusik,A., Hupalowska,A., Voet,T., Marioni,J.C. and Zernicka-Goetz,M. (2016) Heterogeneity in Oct4 and Sox2 targets biases cell fate in 4-cell mouse embryos. *Cell*, **165**, 61–74.
28. Torres-Padilla,M.E., Parfitt,D.E., Kouzarides,T. and Zernicka-Goetz,M. (2007) Histone arginine methylation regulates pluripotency in the early mouse embryo. *Nature*, **445**, 214–218.
29. Zhao,H.Y., Zhang,Y.J., Dai,H., Zhang,Y. and Shen,Y.F. (2011) CARM1 mediates modulation of Sox2. *PloS One*, **6**, e27026.
30. Tee,W.W., Pardo,M., Theunissen,T.W., Yu,L., Choudhary,J.S., Hajkova,P. and Surani,M.A. (2010) Prmt5 is essential for early mouse development and acts in the cytoplasm to maintain ES cell pluripotency. *Genes Dev.*, **24**, 2772–2777.
31. Lee,Y.H., Ma,H., Tan,T.Z., Ng,S.S., Soong,R., Mori,S., Fu,X.Y., Zernicka-Goetz,M. and Wu,Q. (2012) Protein arginine methyltransferase 6 regulates embryonic stem cell identity. *Stem. Cell Dev.*, **21**, 2613–2622.
32. Bedford,M.T. and Clarke,S.G. (2009) Protein arginine methylation in mammals: who, what, and why. *Mol. Cell*, **33**, 1–13.
33. Simandi,Z., Czipa,E., Horvath,A., Koszeghy,A., Bordas,C., Poliska,S., Juhasz,I., Imre,L., Szabo,G., Dezso,B. *et al.* (2015) PRMT1 and PRMT8 regulate retinoic acid-dependent neuronal differentiation with implications to neuropathology. *Stem Cells (Dayton, Ohio)*, **33**, 726–741.
34. Pawlak,M.R., Scherer,C.A., Chen,J., Roshon,M.J. and Ruley,H.E. (2000) Arginine N-methyltransferase 1 is required for early postimplantation mouse development, but cells deficient in the enzyme are viable. *Mol. Cell Biol.*, **20**, 4859–4869.

35. Cai,Y., Yang,G.H. and Zhang,Y. (2015) Establishment of Prmt1 knockout mouse embryonic stem cell lines using the CRISPR-Cas9 system. *J. Med. Res.*, **44**, 18–22.
36. Niakan,K.K., Schrode,N., Cho,L.T. and Hadjantonakis,A.K. (2013) Derivation of extraembryonic endoderm stem (XEN) cells from mouse embryos and embryonic stem cells. *Nat. Prot.*, **8**, 1028–1041.
37. Huang,Y., Pettitt,S.J., Guo,G., Liu,G., Li,M.A., Yang,F. and Bradley,A. (2012) Isolation of homozygous mutant mouse embryonic stem cells using a dual selection system. *Nucleic Acids Res.*, **40**, e21.
38. Saiz,N., Kang,M., Schrode,N., Lou,X. and Hadjantonakis,A.K. (2016) Quantitative analysis of protein expression to study lineage specification in mouse preimplantation embryos. *J. Vis. Exp.*, **108**, 53654.
39. Cheng,M.B., Zhang,Y., Cao,C.Y., Zhang,W.L., Zhang,Y. and Shen,Y.F. (2014) Specific phosphorylation of histone demethylase KDM3A determines target gene expression in response to heat shock. *PLoS Biol.*, **12**, e1002026.
40. Dobin,A., Davis,C.A., Schlesinger,F., Drenkow,J., Zaleski,C., Jha,S., Batut,P., Chaisson,M. and Gingeras,T.R. (2013) STAR: ultrafast universal RNA-seq aligner. *Bioinformatics*, **29**, 15–21.
41. Langfelder,P. and Horvath,S. (2008) WGCNA: an R package for weighted correlation network analysis. *BMC Bioinformatics*, **9**, 559.
42. Trapnell,C., Cacchiarelli,D., Grimsby,J., Pokharel,P., Li,S., Morse,M., Lennon,N.J., Livak,K.J., Mikkelsen,T.S. and Rinn,J.L. (2014) The dynamics and regulators of cell fate decisions are revealed by pseudotemporal ordering of single cells. *Nat. Biotechnol.*, **32**, 381–386.
43. La Manno,G., Soldatov,R., Zeisel,A., Braun,E., Hochgerner,H., Petukhov,V., Lidschreiber,K., Kastriti,M.E., Lonnerberg,P., Furlan,A. *et al.* (2018) RNA velocity of single cells. *Nature*, **560**, 494–498.
44. Klein,A.M., Mazutis,L., Akartuna,I., Tallapragada,N., Veres,A., Li,V., Peshkin,L., Weitz,D.A. and Kirschner,M.W. (2015) Droplet barcoding for single-cell transcriptomics applied to embryonic stem cells. *Cell*, **161**, 1187–1201.
45. Macosko,E.Z., Basu,A., Satija,R., Nemesh,J., Shekhar,K., Goldman,M., Tirosh,I., Bialas,A.R., Kamitaki,N., Martersteck,E.M. *et al.* (2015) Highly parallel Genome-wide expression profiling of individual cells using nanoliter droplets. *Cell*, **161**, 1202–1214.
46. Plass,M., Solana,J., Wolf,F.A., Ayoub,S., Misios,A., Glazar,P., Obermayer,B., Theis,F.J., Kocks,C. and Rajewsky,N. (2018) Cell type atlas and lineage tree of a whole complex animal by single-cell transcriptomics. *Science*, **360**, eaaq1723.
47. Svensson,V. and Pachter,L. (2018) RNA velocity: molecular kinetics from single-cell RNA-Seq. *Mol. Cell*, **72**, 7–9.
48. Kunath,T., Arnaud,D., Uy,G.D., Okamoto,I., Chureau,C., Yamanaka,Y., Heard,E., Gardner,R.L., Avner,P. and Rossant,J. (2005) Imprinted X-inactivation in extra-embryonic endoderm cell lines from mouse blastocysts. *Development (Cambridge, England)*, **132**, 1649–1661.
49. Debeb,B.G., Galat,V., Epple-Farmer,J., Iannaccone,S., Woodward,W.A., Bader,M., Iannaccone,P. and Binas,B. (2009) Isolation of Oct4-expressing extraembryonic endoderm precursor cell lines. *PLoS One*, **4**, e7216.
50. Zhang,X. and Cheng,X. (2003) Structure of the predominant protein arginine methyltransferase PRMT1 and analysis of its binding to substrate peptides. *Structure*, **11**, 509–520.
51. Yan,L., Yan,C., Qian,K., Su,H., Kofsky-Wofford,S.A., Lee,W.C., Zhao,X., Ho,M.C., Ivanov,I. and Zheng,Y.G. (2014) Diamidine compounds for selective inhibition of protein arginine methyltransferase 1. *J. Med. Chem.*, **57**, 2611–2622.
52. Takahashi,K. and Yamanaka,S. (2006) Induction of pluripotent stem cells from mouse embryonic and adult fibroblast cultures by defined factors. *Cell*, **126**, 663–676.
53. Takahashi,K., Tanabe,K., Ohnuki,M., Narita,M., Ichisaka,T., Tomoda,K. and Yamanaka,S. (2007) Induction of pluripotent stem cells from adult human fibroblasts by defined factors. *Cell*, **131**, 861–872.
54. Bialkowska,A.B., Yang,V.W. and Mallipattu,S.K. (2017) Kruppel-like factors in mammalian stem cells and development. *Development (Cambridge, England)*, **144**, 737–754.
55. Aksoy,I., Giudice,V., Delahaye,E., Wianny,F., Aubry,M., Mure,M., Chen,J., Jauch,R., Bogu,G.K., Nolden,T. *et al.* (2014) Klf4 and Klf5 differentially inhibit mesoderm and endoderm differentiation in embryonic stem cells. *Nat. Commun.*, **5**, 3719.
56. Biggar,K.K. and Li,S.S. (2015) Non-histone protein methylation as a regulator of cellular signalling and function. *Nat. Rev. Mol. Cell Biol.*, **16**, 5–17.
57. Blanc,R.S., Vogel,G., Li,X., Yu,Z., Li,S. and Richard,S. (2017) Arginine methylation by PRMT1 regulates muscle stem cell fate. *Mol. Cell. Biol.*, **37**, e00457–00416.
58. Takaoka,K. and Hamada,H. (2012) Cell fate decisions and axis determination in the early mouse embryo. *Development (Cambridge, England)*, **139**, 3–14.
59. Strahl,B.D., Briggs,S.D., Brame,C.J., Caldwell,J.A., Koh,S.S., Ma,H., Cook,R.G., Shabanowitz,J., Hunt,D.F., Stallcup,M.R. *et al.* (2001) Methylation of histone H4 at arginine 3 occurs in vivo and is mediated by the nuclear receptor coactivator PRMT1. *Curr. Biol.*, **11**, 996–1000.
60. Wang,H., Huang,Z.Q., Xia,L., Feng,Q., Erdjument-Bromage,H., Strahl,B.D., Briggs,S.D., Allis,C.D., Wong,J., Tempst,P. *et al.* (2001) Methylation of histone H4 at arginine 3 facilitating transcriptional activation by nuclear hormone receptor. *Science*, **293**, 853–857.
61. Liu,L.M., Sun,W.Z., Fan,X.Z., Xu,Y.L., Cheng,M.B. and Zhang,Y. (2019) Methylation of C/EBPalpha by PRMT1 inhibits its tumor-suppressive function in breast cancer. *Cancer Res.*, **79**, 2865–2877.
62. Yamagata,K., Daitoku,H., Takahashi,Y., Namiki,K., Hisatake,K., Kako,K., Mukai,H., Kasuya,Y. and Fukamizu,A. (2008) Arginine methylation of FOXO transcription factors inhibits their phosphorylation by Akt. *Mol. Cell*, **32**, 221–231.
63. Zhao,X., Jankovic,V., Gural,A., Huang,G., Pardanani,A., Menendez,S., Zhang,J., Dunne,R., Xiao,A., Erdjument-Bromage,H. *et al.* (2008) Methylation of RUNX1 by PRMT1 abrogates SIN3A binding and potentiates its transcriptional activity. *Genes Dev.*, **22**, 640–653.
64. Lin,S.C., Wani,M.A., Whitsett,J.A. and Wells,J.M. (2010) Klf5 regulates lineage formation in the pre-implantation mouse embryo. *Development (Cambridge, England)*, **137**, 3953–3963.
65. Blakeley,P., Fogarty,N.M., Del Valle,I., Wamaitha,S.E., Hu,T.X., Elder,K., Snell,P., Christie,L., Robson,P. and Niakan,K.K. (2015) Defining the three cell lineages of the human blastocyst by single-cell RNA-seq. *Development (Cambridge, England)*, **142**, 3613.
66. Azami,T., Waku,T., Matsumoto,K., Jeon,H., Muratani,M., Kawashima,A., Yanagisawa,J., Manabe,I., Nagai,R., Kunath,T. *et al.* (2017) Klf5 maintains the balance of primitive endoderm versus epiblast specification during mouse embryonic development by suppression of Fgf4. *Development (Cambridge, England)*, **144**, 3706–3718.
67. Hu,D., Gur,M., Zhou,Z., Gamper,A., Hung,M.C., Fujita,N., Lan,L., Bahar,I. and Wan,Y. (2015) Interplay between arginine methylation and ubiquitylation regulates KLF4-mediated genome stability and carcinogenesis. *Nat. Commun.*, **6**, 8419.
68. Cho,L.T., Wamaitha,S.E., Tsai,I.J., Artus,J., Sherwood,R.I., Pedersen,R.A., Hadjantonakis,A.K. and Niakan,K.K. (2012) Conversion from mouse embryonic to extra-embryonic endoderm stem cells reveals distinct differentiation capacities of pluripotent stem cell states. *Development (Cambridge, England)*, **139**, 2866–2877.
69. Zhao,T., Fu,Y., Zhu,J., Liu,Y., Zhang,Q., Yi,Z., Chen,S., Jiao,Z., Xu,X., Xu,J. *et al.* (2018) Single-Cell RNA-Seq reveals dynamic early embryonic-like programs during chemical reprogramming. *Cell Stem. Cell*, **23**, 31–45.
70. Zhao,Y., Zhao,T., Guan,J., Zhang,X., Fu,Y., Ye,J., Zhu,J., Meng,G., Ge,J., Yang,S. *et al.* (2015) A XEN-like state bridges somatic cells to pluripotency during chemical reprogramming. *Cell*, **163**, 1678–1691.